Elevating Growth Factor Responsiveness and Axon Regeneration by Modulating Presynaptic Inputs

Yiling Zhang[1,5], **Philip R. Williams**[1,2,5,6,*], **Anne Jacobi**[1], **Chen Wang**[1], **Anurag Goel**[2], **Arlene A. Hirano**[3], **Nicholas C. Brecha**[4], **Daniel Kerschensteiner**[2], **Zhigang He**[1]

[1]F.M. Kirby Neurobiology Center, Children's Hospital, and Department of Neurology, Harvard Medical School, Boston, USA.

[2]Department of Ophthalmology and Visual Sciences, Washington University School of Medicine, St. Louis, USA.

[3]Department of Neurobiology, Geffen School of Medicine at UCLA, Los Angeles, CA 90095, U.S.A., VAGLAHS, Los Angeles, CA 90073, USA.

[4]Department of Neurobiology, Ophthalmology and Medicine, David Geffen School of Medicine at UCLA, University of California at Los Angeles, Los Angeles, United States Veterans Administration Greater Los Angeles Healthcare System, Los Angeles, USA.

[5]These authors contributed equally

[6]Lead contact

SUMMARY

Despite robust effects on immature neurons, growth factors minimally promote axon regeneration in the adult central nervous system (CNS). Attempting to improve growth factor responsiveness in mature neurons by dedifferentiation, we over-expressed Lin28 in the retina. Lin28 treated retinas responded to insulin-like growth factor-1 (IGF1) by initiating retinal ganglion cell (RGC) axon regeneration after axotomy. Surprisingly, this effect was cell non-autonomous. Lin28 expression was required only in amacrine cells, inhibitory neurons that innervate RGCs. Ultimately, we found that optic nerve crush pathologically upregulated activity in amacrine cells, which reduced RGC electrical activity and suppressed growth factor signaling. Silencing amacrine cells, or pharmacologically blocking inhibitory neurotransmission also induced IGF1 competence. Remarkably, RGCs regenerating across these manipulations localized IGF1 receptor to theirprimary cilia, which maintained their signaling competence and regenerative ability. Thus, our

[*]Correspondence: prwillia@wustl.edu (P.R.W.).

results reveal a circuit-based mechanism that regulates CNS axon regeneration and implicate primary cilia as a regenerative signaling hub.

INTRODUCTION

Since cellular growth is essential for regeneration, external growth-promoting factors in the local environment provide the primary driving force for regeneration. Thus, the availability of growth factors, and the cellular responsiveness to these factors, are critical for dictating the regenerative ability of a cell or tissue. Attempts to regenerate damaged and diseased axons using neurotrophic growth factors have been primarily unsuccessful (Thoenen and Sendtner, 2002). An underlying confound for growth factor application is that, in contrast to immature neurons, mature neurons are regeneration-incompetent and often exhibit decreased responsiveness to growth factors (Duan et al., 2015; Goldberg et al., 2002), which is even further diminished by injury (Belin et al., 2015; Shen et al., 1999). In principle, any step along the course of signal initiation and transduction (e.g. receptor availability, signal propagation, or silencing inhibitory pathways) could be targeted to improve neuronal responsiveness to growth factors. In this regard, activation of the downstream effector of multiple growth factor cascades PI3K/mTOR, by deletion of its negative regulator PTEN, in adult cortical neurons and RGCs is able to promote robust axon regeneration after injury even in the absence of growth factors (Liu et al., 2010; Park et al., 2008; Zukor et al., 2013).

Intriguingly, reduced responsiveness to extracellular factors appears to be a common feature for aging cells and in extreme cases of metabolic dysfunction like type II diabetes, in which the cells in aging organisms lose insulin signaling capacity (Goldstein, 2002). Recent studies demonstrated that in mice, over-expression of Lin28, a heterochronic gene initially identified in *C. elegans* (Ambros, 1989; Ambros and Horvitz, 1984), promotes an insulin-sensitized state that resists high-fat-diet induced diabetes, and removes let-7 mediated inhibition of insulin and insulin like growth factor receptor (IGFR) family expression (Zhu et al., 2011), suggesting an avenue for manipulating cellular responses to extracellular factors. Additionally, Lin28 on its own has been shown to regrow various tissues including skin, hair and digits (Shyh-Chang et al., 2013), along with modest regeneration of RGC axons after optic nerve crush (Wang et al., 2018).

Herein, we demonstrate that Lin28 overexpression in the retina increases RGC survival and allows RGCs to respond to growth factors by mounting a regenerative response following optic nerve crush. Interestingly, this effect was not cell intrinsic as Lin28 was required in amacrine cells and not RGCs. Indeed, examining the amacrine cell response to optic nerve crush, we found that amacrine cells become hyperactivated following RGC injury. Reducing amacrine cell presynaptic inhibition of RGCs, either virally or pharmacologically, similarly promoted RGC survival and growth factor responsiveness. Notably, we discovered that the primary cilia was a point of convergence for amacrine cell silencing mediated RGC regeneration. In RGCs, IGF1R expression is concentrated in primary cilia, this localization is lost after optic nerve crush. Amacrine cell manipulations maintain IGF1R expression in primary cilia of regenerating RGCs, and removing primary cilia reduced regeneration of

treated RGCs. Together, our data show that growth factor signaling after cell damage can be negatively regulated by presynaptic neurons.

RESULTS

Lin28 potentiates growth factor responsiveness in injured RGCs

To determine if the Lin28 could promote responsiveness to growth factors, we tested if AAV2-mediated expression of Lin28 in combination with AAV2-IGF1, AAV2-BDNF, or AAV2-NT-3 could potentiate regeneration of RGCs after an optic nerve crush in adult mice. Three weeks after intravitreal virus injection of singular treatments, combination treatments or AAV2-PLAP (placental alkaline phosphatase) as a control (Park et al., 2008), the optic nerve was crushed and after another two weeks, axon regeneration was monitored by intraocular injection of the anterograde axonal tracer Alexafluor555-conjugated cholera toxin subunit B (CTB) (Figure 1A). While mice injected with AAV2-Lin28, AAV2-IGF1 or AAV2-BDNF demonstrated mild RGC regeneration as previously described (Duan et al., 2015; Wang et al., 2018), the combination of Lin28 and IGF1 or BDNF led to robust axon regeneration beyond that seen with any singular treatment (Figures 1B, 1C, S1A and S1B). Lin28 expression in the retina did not potentiate the minimal effects of AAV2-NT-3 delivery (Figures S1C and S1D). Additionally, Lin28 treatment, either alone or in combination with IGF1, significantly reduced the RGC death that normally follows axotomy in that survival roughly doubled relative to PLAP treated controls at two weeks after injury, while AAV2-IGF1 treatment alone had no survival-promoting effects (Figures 1D and 1E). Since axon regeneration was better potentiated in combination with IGF1, our subsequent experiments focused on IGF1 and not BDNF or NT-3.

Lin28 mediated RGC survival and IGF1 dependent regeneration are not cell intrinsic

Lin28 is not expressed in mature retina (not shown), and intravitreal injection of AAV2-CAG-Lin28 resulted in transgene expression, visualized by immunostaining with antibodies against Lin28, in RGCs as well as two populations of upstream primarily inhibitory interneurons, amacrine and horizontal cells (Figures 2A, 2B and S2). To determine if IGF1 signaling potentiation by Lin28 was cell-intrinsic, we restricted its expression to RGCs using Vglut2-Cre transgenic mice (Ellis et al., 2016). We expressed Lin28 only in RGCs by co-injecting AAV2-FLEX-Lin28 into the vitreous bodies of Vglut2-Cre transgenic mice (Figures 2C and 2D). Surprisingly, while selective expression of Lin28 in RGCs alone recapitulated the modest regenerative effects seen with non-restricted expression, the combination of RGC specific Lin28 expression and widespread IGF1 showed no further increase in regeneration (Figures 2E and 2F). Importantly, such a result indicates that the effects of Lin28 and IGF1 observed with broad overexpression (Figures 1B and 1C) are not likely additive since both individual responses could be observed in Vglut2-Cre mice. Furthermore, AAV2-FLEX-Lin28 into Vglut2-Cre mice also failed to promote RGC survival (Figure 2G).

Since Lin28 expression in RGCs did not induce IGF1 responsiveness, we then used a transgenic line that expresses Cre selectively in inhibitory amacrine and horizontal cells (Vgat-Cre (Vong et al., 2011); Figures 3A and 3B) to target the remaining cellular cohorts

that are transduced by AAV2 intravitreal injection (Figure 2B). Co-injection of AAV2-FLEX-Lin28 and AAV2-IGF1 into Vgat-Cre mice led to robust axon regeneration (Figure 3D), similar to that seen with broad expression of Lin28 (Figures 1B and 1C). Likewise, RGC survival was roughly doubled relative to controls, independent of IGF1 (Figure 3E). Thus, expressing Lin28 selectively in inhibitory neurons presynaptic to RGCs, but not RGCs themselves, promoted a robust regenerative response to IGF1 treatment along with IGF1-independent RGC survival.

Even though fewer horizontal cells than amacrine cells are transduced by AAV2 injection, and horizontal cells do not make direct contact with RGCs, we tested their possible contribution to RGC survival and regeneration. Therefore, we used Cx57-Cre transgenic mice, in which Cre expression is limited to horizontal cells (Hirano et al., 2016). Co-injection of AAV2-FLEX-Lin28 and AAV2-IGF1 into Cx57-Cre mice did not significantly increase RGC axon regeneration or survival relative to the minimal regeneration observed with AAV2-IGF1 alone (Figure S2). Thus, it is likely that the robust neuronal survival and IGF1-dependent axon regeneration observed in Vgat-Cre mice were mainly due to effects on amacrine cells.

Optic nerve crush leads to amacrine cell hyperactivation

As Lin28 can reprogram cell metabolism (Shyh-Chang et al., 2013; Zhu et al., 2011) and has been shown to induce modest axon regeneration on its own (Wang et al., 2018), non-cell autonomous effects on growth factor responsiveness came as a surprise. RGC activity is reduced after axotomy (Stutzki et al., 2014), but it is unknown if this is a cell intrinsic response or resultant to changes in presynaptic activity. Thus, we explored whether optic nerve injury might impact amacrine cell neuronal activity by monitoring expression of an immediate early gene, c-fos, which is an established surrogate for neuronal activity (Sheng and Greenberg, 1990), that has been used in the retina to label active neurons for more than two decades (Yoshida et al., 1993; Hanzlicek et al., 2004). In intact mice that were dark adapted, expression of c-fos in amacrine cells was relatively low (Figure 4A). However, beginning 24 hours after injury, c-fos expression in amacrine cells was significantly upregulated, and remained so for at least one week (Figures 4A and 4B). While c-fos upregulation after injury was primarily seen in amacrine cells, other cells in the inner nuclear layer were also c-fos positive although RGCs and photoreceptors remained primarily negative. Vgat-Cre-dependent Lin28 over-expression significantly reduced the injury-induced expression of c-fos in the lower inner nuclear layer where amacrine cells make up the vast majority of neurons (Figures 4C and 4D). Thus, perhaps by homeostatic mechanisms, amacrine cells appear to become hyperactive in response to the injury of RGC axons, and this hyperactivity is reduced by selective Lin28 expression in amacrine cells.

Blocking amacrine cell synaptic inhibition promotes RGC survival and IGF1 dependent regeneration

Since Lin28 is a factor used to induce pluripotency cells in differentiated cells (Wu et al., 2009; Yu et al., 2007), a possibility is that it reverts amacrine cells to an immature state, reducing their activity and ultimately diminishing inhibitory tone onto RGCs. To examine how Lin28 might lead to reductions in amacrine cell electrical activity, we examined mRNA

levels of a set of neuronal genes 3 weeks after injection of AAV2-FLEX-Lin28/GFP into Vgat-Cre mice against AAV2-FLEX-GFP only controls. Isolated GFP positive cells were collected by FACs sorting and mRNA purified for ddPCR analysis of the following genes: GABRA1, GABRB3, GRIK1, KCNE2, and KCNH6. All mRNA transcripts were downregulated in Lin28 expressing amacrine cells, some significantly so (Figure S4). As such, we postulate that amacrine cell hyperactivity was suppressed in part by a loss of neuronal character.

Reduced amacrine cell inhibition would lead to more activity in RGCs. As such, we compared RGC electrical activity in control (AAV2-FLEX-PLAP in Vgat-Cre mice) and Lin28 treated (AAV2-FLEX-Lin28 in Vgat-Cre mice), injured retinas using multielectrode array recordings of retinal wholemounts. To do this, freshly dissected dark-adapted retinas were subjected to extracellular action potential recordings with 252-electrode arrays, which mainly record RGC-derived electrical signals (Pearson and Kerschensteiner, 2015). We analyzed both spontaneous activity before light exposure and visual stimulation-evoked responses to a white noise stimulus of constant field luminance. In Vgat-Cre retinas with prior optic nerve injury, Lin28 expression in amacrine cells significantly increased spontaneous RGC activity relative to PLAP controls (0.59 +/−.11 Hz in PLAP vs. 3.08 +/− 0.29 Hz in Lin28, p < 0.001, Figures 4E and 4F). We also observed higher RGC firing rates during light stimulation (1.72 +/− 0.20 Hz in PLAP vs. 5.32 +/− 0.41 Hz in Lin28, p < 0.001, Figures 4E, 4G, S4J and S4K). Breakdown of RGC subtypes into ON, OFF and ON-OFF showed that all three subtypes of RGCs fired significantly more with Lin28 expression in amacrine cells (Figure S4A–4C). In spite of this increase in activity, spatiotemporal receptive fields of RGCs, as constructed from spike triggered averages of white noise, were not significantly changed in Lin28-treated retinas, and latency to spike following optimal stimulation was also not changed (Figures S3D–3I). Together, these results suggest that after optic nerve crush, amacrine cells suppress RGC activity, and this hyperinhibition can be reversed by Lin28 expression in amacrine cells.

Since Lin28-mediated RGC regeneration appeared to act by increasing RGC activity through disinhibition, we next asked if RGC activity itself was a necessary component for the Lin28-mediated regenerative response. To do this, we silenced RGCs by selectively expressing the inward rectifying channel Kir2.1 and examined whether Lin28 expression was still able to promote IGF1-elicited axon regeneration (Vglut2-Cre mice treated with AAV2-CAG-IGF1/Lin28 to induce regeneration and AAV2-FLEX-Kir2.1 to silence only RGCs, Figure 5A). We found that Kir2.1 expression specifically in RGCs completely abolished the regeneration phenotypes induced by non-selective Lin28 and IGF1 co-expression (Figures 5B, 5C, 1B and 1C). Overall, these results support a model by which amacrine cell hyperactivity after optic nerve crush suppresses RGCs, preventing their response to growth factors. Amacrine cell treatment with Lin28 reverses this hyperinhibition, and in turn RGC activity is increased along with subsequent survival and IGF1 responsiveness.

To demonstrate that amacrine cell activity modulation itself allows for IGF1 responsiveness, we directly reduced amacrine cell activity by expressing Kir2.1 in amacrine cells (AAV-FLEX-Kir2.1 into Vgat-Cre mice) and examined RGC regeneration when paired with

AAV2-IGF1. With AAV2-FLEX-Kir2.1 alone, we did not observe significant long-distance optic nerve regeneration. In contrast, the combination of AAV2-IGF1 and AAV2-FLEX-Kir2.1 led to robust axon regeneration (Figures 5D–5F). Moreover, inhibition of amacrine cell activity, either alone or in combination with IGF1, significantly increased RGC cell survival (Figure 5G). Thus, silencing amacrine cells, which also led to significantly more spontaneous RGC activity after injury (0.59 +/− .11 Hz in PLAP vs. 0.93 +/− 0.20 Hz Kir2.1, 108 cells 5 mice and Kir2.1, 63 cells 5 mice respectively, $p < 0.05$), was sufficient to allow for IGF1-independent RGC survival and IGF1-dependent axon regeneration after injury. While these alterations in activity might seem modest, similar reductions in firing have been previously implicated in homeostatic changes in the CNS (Burrone et al., 2002)

The results above suggested that reducing presynaptic inhibition onto RGCs results in elevated RGC responsiveness to IGF1. To demonstrate that this was indeed the result of reduced inhibitory neurotransmitter signaling, we used a cocktail of drugs to block inhibitory neurotransmitter receptors present on RGC dendrites and bipolar cell axon terminals. Inhibitory signals onto RGC dendrites are primarily mediated by GABA-A and glycine receptors (Grunert, 2000; Tauck et al., 1988), which we blocked with bicuculline and strychnine respectively. Further, amacrine cells form inhibitory synapses onto bipolar cell axon terminals, which are mainly mediated by glycine and GABA-C receptors (Grunert, 2000; Lukasiewicz et al., 1994; Suzuki et al., 1990; Vaquero and de la Villa, 1999) that can be blocked by 4-imidazoleacetic acid. Thus, a drug cocktail consisting of bicuculline, strychnine and 4-imidazoleacetc acid was injected, with or without IGF1 protein, every three days for two weeks after crush (Figure S5A). Although controls demonstrated some spontaneous regeneration, likely due to increased inflammation caused by repeated intraoccular injections, the antagonist cocktail alone did not enhance long distance optic nerve regeneration compared to vehicle controls, but did significantly increase RGC survival (Figures S5). Furthermore, axonal regeneration induced by combining the inhibitory receptor antagonist cocktail with IGF1 was significantly greater than either treatment alone (Figures S5B–5E). Thus, after RGC axotomy, synaptic inhibition mediated by amacrine cells prevents RGC growth factor responsiveness. Importantly, blocking such inhibition by both genetic and pharmacological means was able to restore RGC responses to IGF1, enabling IGF1-induced axon regeneration.

IGF1R is enriched in healthy RGC primary cilia and is lost after injury

Next, we explored the mechanism by which amacrine cell activity affected IGF1 responsiveness of RGCs. We first examined the expression of IGF1 receptor (IGF1R) protein by immunofluorescence with an anti-IGF1R antibody characterized previously in the CNS (Hollis et al., 2009; Liu et al., 2017). IGF1R immunoreactivity was localized to puncta throughout the thickness of all retinal layers and could be localized to multiple cell types (not shown). Strikingly, on RGC somata, IGF1R signal was concentrated in what appear to be primary cilia (Figure 6A–6C). This localization was verified by demonstrating that IGF1R immunoreactivity was adjacent to and contiguous with pericentrin (Figure 6B), a marker of the ciliary rootlet (Jurczyk et al., 2004). Antibody specificity was confirmed by absence of cilia staining in a Cre dependent IGF1R knockout mouse (Figure S6A). From wholemount samples (Figure 6A), it appeared that most, if not all, RGCs have IGF1R

immunoreactivity enriched in their cilia, whereas other retinal cells with this feature are rare. In cross sections, 90.2 +/− 0.1% of RGCs (n = 470 RGCs, 7 mice) possess single primary cilia with detectable IGF1R signals (Figures 6B and 6C), likely because cryosections leave portions of RGCs that lack cilia on their edges..

Despite the documented role of primary cilia as a signaling center during development (Guemez-Gamboa et al., 2014; Hilgendorf et al., 2016), their role in mature neurons has not been well characterized (Siljee et al., 2018). Examining the expression of IGF1R in RGC cilia after axotomy, we found that by 7 days after optic nerve crush, IGF1R immunoreactivity in RGC cilia was mostly lost (Figures 6C and 6D). This was not due to a loss of cilia in RGCs, as the cilia marker adenylate cyclase III (Bishop et al., 2007) continued to label RGC cilia at this time point (Figures 6E and 6F), although cilia were somewhat shortened in response to injury (2.26 +/− 0.05 μm, 1.67 +/− 0.05 μm and 1.41 +/− 0.04 μm in uninjured, 3 and 7 day post crush respectively). Loss of IGF1R from primary cilia was also not due to suppression of activity in RGCs as injection of AAV2-FLEX-Kir2.1 into Vglut2-Cre mice to silence RGCs without injury did not alter IGF1R localization (Figure S6B). Importantly, when Lin28 or Kir2.1 was expressed specifically in amacrine cells, significantly more RGCs maintained IGF1R expression in their cilia (Figures 6G and 6H). Thus, diminishing amacrine cell activity maintained detectable IGF1R expression in the primary cilia of a portion of surviving RGCs.

Since Lin28 promoted BDNF mediated axon regeneration, we also examined if BDNF signaling might involve primary cilia localization of the receptor TrkB, but although it localized to photoreceptor inner segments, we did not notice ciliary localization in RGCs (Figure S6C). Taken together with the smaller combinatorial effects of Lin28 and BDNF, we believe the increased regeneration might be due to additive effects.

Regenerating RGCs maintain IGF1R in their primary cilia

To distinguish between regenerating and surviving RGCs, we labeled RGCs possessing long-distance regenerating axons with a retrograde tracer, 3kD dextran conjugated to biotin, which was applied to a freshly severed optic nerve stump approximately 1.5 mm distal to the original crush (Figures 7A and 7B). While such labeling efficiently tagged the vast majority of RGCs in the intact retina, tracing after optic nerve crush did not label RGCs in non-regenerating control retinas (not shown). Backtracing in Vgat-Cre mice that were treated with AAV2-FLEX-Lin28 and AAV2-IGF1, 4 weeks after optic nerve crush led to labeling almost exclusively in Rbpms-positive RGCs (Figures 7C–7E). Importantly, most of these labeled RGCs had IGF1R immunoreactive cilia (Figures 7C and 7F), and were positive for pS6 (Figures 7D and 7F), indicating activation of the mTOR pathway that is downstream of IGF1R signaling. Thus, our results suggest the localization of IGF1R in the primary cilia of adult RGCs represents a key mechanism for their regenerative competency. Decreasing injury induced hyperactivity of amacrine cells *via* Lin28 or Kir2.1 overexpression, maintains IGF1R expression in some RGC primary cilia, and ultimately allows them to respond to growth factor treatments and mount a regenerative response.

To examine the RGC subtype specificity of this response, we also immunostained backtraced samples for the alpha-RGC marker osteopontin-1 (OPN1) and found that a

majority of regenerating RGC were alpha-RGCs (Figure 7E and 7F), similar to other regenerative strategies stimulating IGF signaling (Duan et al., 2015). Taken together with the fact that roughly one third of amacrine cells upregulated c-fos after optic nerve crush (Figure 4a) and some amacrine cells subtypes as a whole did not upregulate c-fos (Figure S7), we believe that there is likely an aspect of circuit specificity underlying the regenerative mechanisms resultant from amacrine cell inhibition.

Loss of primary cilia reduces Lin28 mediated regeneration

To test the requirement of IGF1R enrichment in cilia, we conditionally knocked out the critical cilia trafficking protein Intraflagellar transport protein 88 (IFT88), a transport protein of the primary cilia essential for its formation and maintenance (Haycraft et al., 2007). This manipulation has been previously demonstrated to remove cilia from most examined adult neurons in the hypothalamus within 10 days of the onset of tamoxifen induced Cre expression (Berbari et al., 2013). Thus, we injected AAV2-Lin28 and AAV2-IGF1 into IFT88 floxed mice along with AAV2-Cre to induce the knockout of IFT88, or AAV2-PLAP as a control (Figure 7G). IFT88 knockout had no effect on axon regeneration in untreated samples (Figure 7H and 7I), and no effect on RGC survival in either untreated (24.0 +/− 0.3% vs. 24.1 +/− 1.7% in AAV2-PLAP and AAV2-Cre respectively) or treated (41.6 +/− 3.4% vs. 40.4 +/− 3.2% AAV2-PLAP/IGF/Lin28 vs. AAV2-Cre/IGF/Lin28 respectively) conditions. However, although mice with IFT88 knockout induction still demonstrated moderate regeneration, significantly reduced numbers of regenerating axons were detected in mice with IFT88 deletion relative to regenerating controls (Figures 7H and 7I). A partial effect of cilia removal is not entirely surprising given that Lin28 itself demonstrated a modest amount of regeneration without IGF1 (Figures 1B and 1C), IGF1R located on RGCs away from the primary cilia can likely still mediate some growth factor response (Zhu et al., 2009), and in our hands AAV2-Cre mediated inducible knockout of IFT88 only led to a partial loss of primary cilia and corresponding IGF1R enriched cilia in RGCs (35.4 +/− 4.1% and 44.1 +/− 3.5% reductions respectively). Thus, our results suggest that in RGCs primary cilia play an important role for mediating regenerative responses to IGF1.

DISCUSSION

While available studies have been focused on intrinsic pathways regulating axon growth ability, our results reveal a mechanism that limits neuronal regenerative ability in a non-cell-autonomous manner. We found that axotomy triggers a set of homeostatic alterations in the local network that repress the growth potential of injured neurons. This increase in inhibitory synaptic tone onto RGCs following their axotomy ultimately represents a circuit-level brake preventing RGC axon regeneration, by diminishing their responses to growth factors. Further, the homeostatic changes in injured RGCs that are prevented by amacrine cell silencing also play a role in RGC survival independent of growth factor signaling. Although the amount of regeneration we observed by potentiating IGF1 signaling with amacrine cell silencing was similar to that seen with OPN1 mediated potentiation (Duan et al., 2015), amacrine cell silencing alone doubled survival of axotomized RGCs (Figure 5G), whereas OPN1 mediated IGF1 potentiation did not enhance RGC survival. Thus, we suspect that while OPN1 signaling likely only alters responsiveness to IGF1, amacrine cell silencing may

induce a range of beneficial effects on RGCs in line with treatments that directly increase RGC electrical activity (Li et al., 2016; Lim et al., 2016). Although such beneficial effects seem were most robust for the IGF1 growth factor family (Figure S1).

Importantly, manipulating the activity of amacrine cells or their synaptic connections with RGCs could represent a powerful strategy to regulate RGC growth factor signaling competence, by enhancing their regenerative ability. Indeed, we have demonstrated that a cocktail of inhibitory receptor blockers, some of which have demonstrated human tolerance (Clark, 1938), can improve RGC survival and growth factor responsiveness. Different hypotheses have been posited to explain the role of neuronal activity in the control of axonal growth ability. While several studies have implied a positive role (Goldberg et al., 2002; Li et al., 2016; Lim et al., 2016), a different model holds that the development-dependent transition from axon growth to synaptic transmission regulates the loss of axon growth ability (Cohan and Kater, 1986; Enes et al., 2010; Tedeschi et al., 2016). A possible explanation could be relevant to different innervation patterns of the neurons studied: sensory neurons from dorsal root ganglia that lack presynaptic partners in activity inhibiting studies (Cohan and Kater, 1986; Enes et al., 2010; Tedeschi et al., 2016); and RGCs that have presynaptic partners for studies where axonal regeneration in response to growth factors is potentiated by activity (Goldberg et al., 2002; Li et al., 2016; Lim et al., 2016).

It is quite unexpected that the growth factor competence induced by Lin28 expression in the retina was not cell intrinsic. While we were able to reproduce very modest axon regeneration seen with non-restricted AAV2 treatments (Wang et al., 2018) and Figures 1B, 1C, 2C and 2D), as Lin28 is known to promote IGF signal response (Zhu et al., 2011) we might have expected synergistic effects within RGCs themselves. Indeed, our experiments demonstrate the importance of validating cell intrinsic responses with cell-type restricted gene expression. While often overlooked, gene expression mediated by intravitreal delivery of AAV2 has been documented for quite some time (Martin et al., 2002; McKinnon et al., 2004). Other transcription factors known to play a role in neuronal development have been shown to induce RGC axon regeneration using gene expression or knockdown systems that would presumably express in amacrine cells as well as RGCs (Moore et al., 2009; Norsworthy et al., 2017). Thus, it is possible that suppression of amacrine cell injury induced hyperactivity, similar to Lin28, may underlie some of these observations.

It is striking that IGF1 signaling competence is remarkably dependent on the accumulation of IGF1R in primary cilia of these adult RGCs. Our results suggest that the enrichment of growth factor receptors, and perhaps other signaling molecules, in primary cilia could represent a strategy for amplifying neuronal sensitivity to extracellular growth signals and thus regulate their cellular metabolism and function. Indeed, IGF1R enrichment into primary cilia has been observed over the course of adipocyte differentiation (Zhu et al., 2009). Additionally, recent studies have demonstrated that the receptor for melanocortin-4 (MC4R) is enriched in neuronal primary cilia (Siljee et al., 2018). Interestingly, mutations in genes encoding ciliary proteins such as centrosomal protein 19, ankyrin repeat domain 26, adenylate cyclase 3, and MC4R, have been shown to cause obesity in mice and humans (Acs et al., 2015; Shalata et al., 2013), suggesting an important role of primary cilia as signaling antennae that regulate organismal metabolism and obesity. A mirrored role for regulating the

state of cellular level metabolic state would indicate that ciliary localization of growth factor signaling components could strongly impact an injured neurons growth potential (He and Jin, 2016). Taken together, our results identify a circuit-level brake on axon regeneration that develops upstream of RGCs as a result of their axonal injury. Overcoming this presynaptic inhibition allows for CNS neurons to respond to growth factors, *via* a mechanism that maintains growth factor receptor localization to primary cilia, and subsequent axon regeneration.

STAR*METHODS

CONTACT FOR REAGENT AND RESOURCE SHARING

Further information and requests for reagent will be addressed by the lead author Philip R. Williams (prwillia@wustl.edu).

EXPERIMENTAL MODEL AND SUBJECT DETAILS

Mouse Strains—All experimental procedures were performed in compliance with animal protocols approved by the IACUC at Boston Children's Hospital and Washington University in St. Louis. Mice aged 3–5 weeks at the start of experiments were used throughout. Male and female mice were used in this study at ratios dependent on litters available and with equal distributions across experiments conducted extemporaneously. C57BL6/J, Vglut2-ires-Cre (028863; Jackson Labs), Vgat-IRES-Cre (016962; Jackson Labs), IFT88*fl/fl* (022409; Jackson Labs) and IGF1R*fl/fl* (mouse lines were obtained from Jackson Laboratories. The connexin 57cre (Cx57-Cre) mouse line was described in (Hirano et al., 2016).

Constructs—The AAV-CAG-PLAP, AAV-CAG-IGF1, and AAV-CAG-BDNF expression vectors were previously reported by our lab (Liu et al., 2017). The AAV-CAG-Lin28a expression vector was cloned by bioabl using the pAAV-MCS backbone (Stratagene). The AAVCAG-FLEXLin28a and AAV-CAG-FLEX-Kir2.1 P2A tdTomato were cloned by Vigene Sciences Inc. using the pAAV-MCS and #60661 (Addgene) backbones respectively.

Antibodies—Primary antibodies used were: Rabbit anti-Lin28 (1:500, Cell signaling, 3978); Mouse antiLin28 (1:500, Cell Signaling, 5930); Guinea pig anti-RBPMS (1:2000, Raygene A008712); Rabbit anti-c-Fos (1:500, Cell Signaling, 2250); Rabbit anti-IGF1R ((*31, 33*) 1:500, Santa Cruz, sc-712), rabbit anti-AP2 (1:200, Abcam, 52222), mouse anti-AP2 (1:50, Developmental Studies Hybridoma Bank, 3B5), rabbit anti-pericentrin (1:500, Biolegend, 923701), rabbit anti-adenylate cyclase III (1:500, Thermofisher, PA5–35382) rabbit anti-phospho S6 (1:100, Cell Signaling, 4857), rabbit anti-TrkB (1:20, Thermofisher, PA5–78405), goat anti-osteopontin 1 (1:400x R&D Systems, AF1433), and goat anti-choline acetyl transferase (1:400x Millipore, AB144P). Secondary antibodies were used from Jackson ImmunoResearch or Life Technologies, raised in either goat or donkey against primary antibody's host species, highly cross adsorbed and conjugated to fluorophores of Alexa Fluor 488, Alexa Fluor 568, or Alex Fluor 647, and used at a 1:400–500 dilution. For microruby amplification, streptavidin conjugated to Alexafluor 568 (1:1000, life Technologies, S11226) was used to amplify against the biotin tag.

METHOD DETAILS

Virus Production—Boston Children's Hospital Viral Core provided AAV virus. AAV serotype 2 were used in our study as following: AAV2-PLAP; AAV2-Lin28; AAV2-IGF1; AAV2-BDNF; AAV2-FlexPLAP; AAV2-Flex-Lin28; AAV2-Flex-Kir2.1; AAV2-Flex-GFP; AAV2-Cre. The titers of all viral preparations were at least 1.0×10^{13} GC/mL.

Surgical Procedures—For all surgical procedures mice were anaesthetized with ketamine and xylazine and received Buprenorphine as a postoperative analgesic.

<u>**AAV Virus Injections:**</u> For intravitreal injections, a pulled-glass micropipette was inserted near peripheral retina behind the ora serrata and deliberately angled to avoid damage to the lens. 2–3 μl of AAV were injected intravitreally. When two viruses were injected, viruses were pre-mixed to appropriate concentrations and injected in the same volume.

<u>**Drug Injections:**</u> A cocktail of inhibitory neurotransmitter receptors (3.33 mM bicuculline, 6.66 mM 4-imidazoleacetic acid and 0.167 mM strychnine in 17% DMSO; all from Sigma, in sterile saline) in 1 μL was injected as described above on the time course indicated in fig. S4. For IGF1 treatment, 1 μg of recombinant human IGF1 was added to the combination of drugs, or injected in the vehicle solution.

<u>**Optic Nerve Injury:**</u> Three weeks after AAV injection, we performed optic nerve injury as previously described (Park et al., 2008). Briefly, the optic nerve was exposed intraorbitally and crushed with fine forceps (Dumont #5 FST) for 5 seconds approximately 500 μm behind the optic disc. Eye ointment was applied post-operatively to protect the cornea.

<u>**Anterograde RGC Labeling:**</u> Two to three days before perfusion, 2 μl cholera toxin subunit B (CTB-Alexfluor555, 2 μg/μl in sterile PBS, ThermoFisher) was injected intravitreally with a pulled glass micropipette attached to a Hamilton syringe (Hamilton).

<u>**Retrograde RGC Labeling:**</u> Retrograde labeling of regenerated RGCs was performed as follows. Four weeks after optic nerve crush, mice were anesthetized and placed in a stereotaxic holder. The crushed optic nerve was exposed using a superior temporal intraorbital approach by drilling through the skull and removing overlaying brain tissue. After exposing the optic nerve approximately 1.5 mm distal to the crush site, we cut the nerve with a fine blade delivered 100–300 nl of 5% microruby (3 kD dextran conjugated to biotin and TRITC; ThermoFisher) solution diluted in sterile PBS was delivered to the stump. We then placed a small piece gelfoam (Fisher Scientific) soaked in 5% microruby on the cut nerve stump. The scalp was sutured and animals recovered on a heating pad until they regained consciousness. Mice were perfused 32 hours after the backtracing surgery.

Perfusions and Tissue Processing—Animals were given an overdose of anesthesia and transcardiacally perfused with ice cold PBS followed by 4% paraformaldehyde (Sigma). For c-fos immunostaining, mice were dark adapted overnight, to limit signal from light evoked activity, given anesthesia under dim room light and perfused under normal room lighting. After perfusion, optic nerves and eye balls were dissected out and post-fixed in 4% PFA overnight at 4°C. Tissues were cryoprotected by sinking in 15% sucrose in PBS for

optic nerves and 30% sucrose for eyes. Samples were frozen in Optimal Cutting Temperature compound (Tissue Tek) using a dry ice and ethanol bath, then sectioned at 14 μm for optic nerves and 20 μm for eyes.

Immunostaining—Immunostaining was performed with the following protocols. All sections were washed with PBS then blocked in a solution of 3% bovine serum albumin (Sigma) or 10% normal donkey serum (Jackson Immunoresearch) and 0.1–0.5% Triton X-100 in PBS for 1 h. Samples were then incubated with primary antibodies diluted in the blocking solution overnight. After being washed three times with PBS, secondary antibodies were applied for 2–3 h at room temperature in blocking solution. After being washed three times, sections were mounted onto glass slides with DAPI-Fluoromount-G (VWR) or Vectashield (Vector Labs).

Microscopy—An Ultraview Vox Spinning Disk confocal microscope (Perkin Elmer) equipped with a 20X air objective was used to acquire image stacks with a 2-μm z spacing and 20% overlap in x-y dimensions of optic nerves to assess axon regeneration and retinas to assess RGC survival. Samples were automatically stitched with Velocity software (Perkin Elmer). For cilia and backtracing experiments, an LSM 710 scanning confocal microscope (Zeiss) equipped with a 20 X air or 63 X oil immersion objective was used to acquire z-stacks at 2.0 m thickness or 0.6 – 1.0 μm thickness respectively. Brightness and contrast of the images were adjusted and pseudo-colored for presentation. Image capture and processing conditions were kept constant when imaging was used for quantification. For display clarification, in images of IGF1R showing cilia, cilia were hand traced in Image J and pseudocolored separately from the rest of IGF1R staining in Figure 4 A, B and D.

Image Analysis—To measure regenerating RGC axons after optic nerve crush, longitudinal sections of optic nerves were serially collected. Regenerating RGC axons were quantified as described previously (Park et al., 2008). CTB labeled axons were estimated by counting the number of CTB labeled fibers extending indicated distances from the crush site across three sections from each nerve to estimate the number of regenerating axons in a biological sample.

All image analysis of the retina was performed on 20 μm thick cryosections. For all analyses, where possible, images were collected at the central third of the retina where RGC transduction rates were highest. Rbpms immunostained samples were used to measure RGC survival after optic nerve crush. RGC numbers were counted from two montaged 20 mm thick retinal sections per animal (approximately 2500–3000 μm per section) using the cell counter plugin from Image J software. In intact retina sections, generally 300 to 400 Rbpms positive cells were counted per section. We calculated the linear density of Rbpms positive cells in the GCL and normalized these counts to a standard control non-injured. We also examined INL thickness, a proxy for amacrine cell survival, in our Lin28 and Kir2.1 amacrine cell expression samples and found no difference between PLAP controls, Lin28 treated or Kir2.1 treated retinas (34.0 +/− 0.7, 35.7 +/− 1.0 and 33.6 +/− 0.6 μm respectively, n = at least 4 mice per group).

To quantify c-fos intensity in amacrine cells, single fields of view from 20 X scanning confocal stacks that were stained with AP-2 and c-fos antibodies were analyzed in ImageJ. ROIs circling amacrine cells based on AP2 staining were used to blindly measure the signal intensity in the c-fos channel. For Lin28 treated samples, the combination of AP2 and c-fos antibodies was not possible, therefore we analyzed c-fos intensity in the 'lower' inner nuclear layer by generating a large ROI across a maximum intensity projected image that contained the 2 – 3 cell bodies proximal to the inner plexiform layer interface using the DAPI channel as a guide.

To quantify IGF1R and ACIII staining, confocal scanning images acquired with the 63 X oil immersion objective were used to first identify presumptive primary cilia and then those contained within or contiguous with an Rpbms positive (or Rbpms and dextran double positive) cell body in the inner plexiform layer were counted along with Rbpms positive cells lacking cilia. When a confocal color channel was available, pericentrin immunostaining was included to aid in identification of primary cilia.

Multielectrode Array (MEA) Recordings—Mice were killed in a CO_2 chamber, and retinas were dissected in ice cold mouse artificial cerebrospinal fluid (125 NaCl, 2.5 KCl, 1.25 Na_2HPO_4, 2 $CaCl_2$, 1 $MgCl_2$, 20 Glucose, 26 $NaHCO_3$, 0.5 L-Glutamine in mM equilibrated with 95% O2 5% CO2) under dim red light. We recorded extracellular action potentials on planar 252-electrode arrays (Multi Channel Systems, electrode size: 10 m, center-center distance: 100 m). During recordings, retinas were perfused at 6 – 8 mL/min with warm (33 °C) mouse artificial cerebrospinal fluid. We bandpass filtered signals of all electrodes (300 – 3,000 Hz), digitized them (10 kHz), and acquired 3-ms cut-outs whenever signals crossed a threshold set manually for each electrode. We then sorted these waveforms into spike trains representing the activity of individual cells using principal component analysis (Offline Sorter, Plexon). We analyzed the cross-correlation of spike trains to detect when one neuron had been recorded on multiple electrodes. In these cases, only the train with the most spikes was used for further analysis.

Visual Stimulation and Analysis—We wrote visual stimuli in Matlab (Mathworks) using the Cogent Graphics toolbox extensions developed by John Romaya at the LON at the Wellcome Department of Imaging Neuroscience, and projected them from an organic light emitting display (OLEDXL, eMagin) through a 20 X 0.5 NA water immersion objective (Olympus) onto the retina. The display output was linearized using custom scripts. In the checkerboard white noise stimulus, the intensity of squares of 50 m side length was chosen at random from a Gaussian distribution every 33 ms (refresh rate: 30 Hz). The mean stimulus intensity was 1,000 rhodopsin isomerizations / rod / s (1,000 R*), and the stimulus contrast (SD / mean) 40%. We used a linear – nonlinear cascade model to describe the light responses of RGCs (Chichilnisky EJ, 2001 and Kerschensteiner et al., 2008). We calculated the linear part of this model, the spatiotemporal receptive field of the RGC, from its spike-triggered stimulus average (STA). To calculate the nonlinear part of the model, the dependence of the RGC activity on the match between the stimulus and the RGC's spatiotemporal receptive field, we convolved the stimulus with the STA. The timevarying output of this convolution is called the generator signal. We split the range of generator

signals into 25 bins and calculated the average spike rate in these bins to complete the model. Linear and nonlinear parts of the model were estimated in separate parts of the recording. To measure an RGC's receptive field size, we fit a 2D Gaussian to the spatial profile at the temporal peak of the STA, and calculated the equivalent radius of the ellipse at 1 SD. To measure response timing of an RGC, we calculated the delay of the temporal peak in the STA. We measured the peak response of an RGC as the average firing rate in its highest generator signal bin.

FACs Sorting and ddPCR—ddPCR was performed in triplicate with 4 retinas combined per sample. FACs sorting was carried out as previously described (Norsworthy et al., 2017). Breifly, Vgat-Cre transgenic mice were deeply anesthetized and decapitated 3 weeks after intraocular injection of either AAV2-FLEX-GFP or AAV2-FLEX-Lin28 and AAV2-FLEX-GFP. Eyeballs were removed and retinas were dissected in chilled Hanks balanced salt solution (HBSS, Life Technologies, 14170–112) with 10 mM HEPES added. 3–4 retinas were pooled per sample into 2 mL of 37°C digestion solution (HBSS with HEPES (Sigma, H3375), 0.032% w/v L-cysteine (Sigma, C7477), 50 μg/mL DNAse (Sigma, D4527), 1U/mL papain (Worthington, LS003126), filtered through a 0.22 mm filter (Millipore, SCGP00525) before adding 40 U/mL Protector RNAse Inhibitor (Roche, 03335399001)). Samples were digested for 4 minutes at 37°C and then centrifuged at 450Xg for 4 min at 4°C. The supernatant was discard ed and cells resuspended in digestion inhibitor (MEM with phenol Red (Life Technologies, 11090-081) containing 1% w/v bovine serum albumin (BSA, Sigma, A2153), 1% w/v trypsin inhibitor from egg white (Sigma, T9253) 50 mg/mL DNAse, filtered through a 0.22 mm filter before adding 20 U/mL Protector RNAse Inhibitor) by titrating up and down 8–10 times as needed. Samples were centrifuged for at 350–400Xg for 40 sec at 4°C, and the supernatant was saved. Pellets were resuspended as before and this process was repeated until only a minimal pellet remained. The collected cells were filtered through a 40 mm cell strainer (Fisher, 08-771-1), centrifuged for at 450Xg for 10 min at 4°C, the supernatant discarded and the pellet resuspended in 1–4 mL of DMEM (Life Technologies, 31053–028) containing 0.4% BSA, 5 U/mL Protector RNAse and 1 mM calcein blue (Sigma, M1255). FACs sorting was performed using a BD FACsAria II Flow Cytometer equipped with a 70 mm nozzle using a filter set for DAPI excitation to screen viable calcein blue positive cells and GFP expressing virally infected cells. Samples were sorted directly into Extraction Buffer from the Arcturus PicoPure RNA Isolation Kit (Thermofisher, KIT0204)

RNA was purified using the Arcturus PicoPure RNA Isolation Kit according to the manufacturers instructions. ddPCR was performed using the One-Step RT-ddPCR Advanced Kit (Bio-RAD, 1864021). ddPCR Expression Probes for Grik1, Gabra1, Gabrb3, Kcnh6 and Kcne2 (Bio-RAD, dMmuCPE5095450, dMmuCPE5118172, dMmuCPE5099818, dMmuCPE5115490, dMmuCPE5113084) were measured according to the manufacturer's instructions and normalized to levels of Tbp (Bio-RAD, dMmuCPE5124759).

STATISTICAL ANALYSIS

One-way ANOVAs with Bonferroni Correction were performed with PRISM software to examine statistical significance of axon regeneration data. Mann-Whitney U-Test was used for two group comparisons. Error bars represent the SEM.

Supplementary Material

Refer to Web version on PubMed Central for supplementary material.

ACKNOWLEGMENTS

REFERENCES

Acs P, Bauer PO, Mayer B, Bera T, Macallister R, Mezey E, and Pastan I (2015). A novel form of ciliopathy underlies hyperphagia and obesity in Ankrd26 knockout mice. Brain Struct Funct 220, 1511–1528. [PubMed: 24633808]

Ambros V (1989). A hierarchy of regulatory genes controls a larva-to-adult developmental switch in C. elegans. Cell 57, 49–57. [PubMed: 2702689]

Ambros V, and Horvitz HR (1984). Heterochronic mutants of the nematode Caenorhabditis elegans. Science 226, 409–416. [PubMed: 6494891]

Belin S, Nawabi H, Wang C, Tang S, Latremoliere A, Warren P, Schorle H, Uncu C, Woolf CJ, He Z, et al. (2015). Injury-induced decline of intrinsic regenerative ability revealed by quantitative proteomics. Neuron 86, 1000–1014. [PubMed: 25937169]

Berbari NF, Pasek RC, Malarkey EB, Yazdi SM, McNair AD, Lewis WR, Nagy TR, Kesterson RA, and Yoder BK (2013). Leptin resistance is a secondary consequence of the obesity in ciliopathy mutant mice. Proc Natl Acad Sci U S A 110, 7796–7801. [PubMed: 23599282]

Bishop GA, Berbari NF, Lewis J, and Mykytyn K (2007). Type III adenylyl cyclase ocalizes to primary cilia throughout the adult mouse brain. J Comp Neurol 505, 562–571. [PubMed: 17924533]

Burrone J, O'Byrne M, and Murthy VN (2002). Multiple forms of synaptic plasticity triggered by selective suppression of activity in individual neurons. Nature 420, 414–418. [PubMed: 12459783]

Chichilnisky EJ (2001). A simple white noise analysis of neuronal light responses. Network: Comput Neural Syst 12, 199–213.

Clark AJ (1938). Applied Pharmacology. (Blakiston's Son and Co. Inc.), pp. 255–259.

Cohan CS, and Kater SB (1986). Suppression of neurite elongation and growth cone motility by electrical activity. Science 232, 1638–1640. [PubMed: 3715470]

Duan X, Qiao M, Bei F, Kim IJ, He Z, and Sanes JR (2015). Subtype-specific regeneration of retinal ganglion cells following axotomy: effects of osteopontin and mTOR signaling. Neuron 85, 1244–1256. [PubMed: 25754821]

Ellis EM, Gauvain G, Sivyer B, and Murphy GJ (2016). Shared and distinct retinal input to the mouse superior colliculus and dorsal lateral geniculate nucleus. J Neurophysiol 116, 602–610. [PubMed: 27169509]

Enes J, Langwieser N, Ruschel J, Carballosa-Gonzalez MM, Klug A, Traut MH, Ylera B, Tahirovic S, Hofmann F, Stein V, et al. (2010). Electrical activity suppresses axon growth through Ca(v)1.2 channels in adult primary sensory neurons. Curr Biol 20, 1154–1164. [PubMed: 20579880]

Goldberg JL, Espinosa JS, Xu Y, Davidson N, Kovacs GT, and Barres BA (2002). Retinal ganglion cells do not extend axons by default: promotion by neurotrophic signaling and electrical activity. Neuron 33, 689–702. [PubMed: 11879647]

Goldstein BJ (2002). Insulin resistance as the core defect in type 2 diabetes mellitus. Am J Cardiol 90, 3G–10G.

Grunert U (2000). Distribution of GABA and glycine receptors on bipolar and ganglion cells in the mammalian retina. Microsc Res Tech 50, 130–140. [PubMed: 10891877]

Guemez-Gamboa, A., Coufal, N.G., and Gleeson, J.G. Primary cilia in the developing and mature brain. Neuron 82, 511–521.Guemez-Gamboa A, Coufal NG, and Gleeson JG (2014). Primary cilia in the developing and mature brain. Neuron 82, 511–521. [PubMed: 24811376]

Hanzlicek BW, Peachey NS, Grimm C, Hagstrom SA, and Ball SL (2004). Probing inner retinal circuits in the rod pathway: A comparison of c-fos activation in mutant mice. Vis Neurosci 21, 873–881. [PubMed: 15733342]

Haycraft CJ, Zhang Q, Song B, Jackson WS, Detloff PJ, Serra R, and Yoder BK (2007). Intraflagellar transport is essential for endochondral bone formation. Development 134, 307–316. [PubMed: 17166921]

He Z, and Jin Y (2016). Intrinsic Control of Axon Regeneration. Neuron 90, 437–451. [PubMed: 27151637]

Hilgendorf KI, Johnson CT, and Jackson PK (2016). The primary cilium as a cellular receiver: organizing ciliary GPCR signaling. Curr Opin Cell Biol 39, 84–92. [PubMed: 26926036]

Hirano AA, Liu X, Boulter J, Grove J, Perez de Sevilla Muller L., Barnes S, and Brecha NC (2016). Targeted Deletion of Vesicular GABA Transporter from Retinal Horizontal Cells Eliminates Feedback Modulation of Photoreceptor Calcium Channels. eNeuro 3.

Hollis ER 2nd, Lu P, Blesch A, and Tuszynski MH (2009). IGF-I gene delivery promotes corticospinal neuronal survival but not regeneration after adult CNS injury. Exp Neurol 215, 53–59. [PubMed: 18938163]

Jurczyk A, Gromley A, Redick S, San Agustin J, Witman G, Pazour GJ, Peters DJ, and Doxsey S (2004). Pericentrin forms a complex with intraflagellar transport proteins and polycystin-2 and is required for primary cilia assembly. J Cell Biol 166, 637–643. [PubMed: 15337773]

Kerschensteiner D, and Wong RO (2008). A precisely timed asynchronous pattern of ON and OFF retinal ganglion cell activity during propagation of retinal waves. Neuron 58, 51–858.

Li S, Yang C, Zhang L, Gao X, Wang X, Liu W, Wang Y, Jiang S, Wong YH, Zhang Y, et al. (2016). Promoting axon regeneration in the adult CNS by modulation of the melanopsin/GPCR signaling. Proc Natl Acad Sci U S A 113, 1937–1942. [PubMed: 26831088]

Lim JH, Stafford BK, Nguyen PL, Lien BV, Wang C, Zukor K, He Z, and Huberman AD (2016). Neural activity promotes long-distance, target-specific regeneration of adult retinal axons. Nat Neurosci 19, 1073–1084. [PubMed: 27399843]

Liu K, Lu Y, Lee JK, Samara R, Willenberg R, Sears-Kraxberger I, Tedeschi A, Park KK, Jin D, Cai B, et al. (2010). PTEN deletion enhances the regenerative ability of adult corticospinal neurons. Nat Neurosci 13, 1075–1081. [PubMed: 20694004]

Liu Y, Wang X, Li W, Zhang Q, Li Y, Zhang Z, Zhu J, Chen B, Williams PR, Zhang Y, et al. (2017). A Sensitized IGF1 Treatment Restores Corticospinal Axon-Dependent Functions. Neuron 95, 817–833 e814. [PubMed: 28817801]

Lukasiewicz PD, Maple BR, and Werblin FS (1994). A novel GABA receptor on bipolar cell terminals in the tiger salamander retina. J Neurosci 14, 1202–1212. [PubMed: 8120620]

Martin KRG, Klein RL, and Quigley HA (2002). Gene delivery to the eye using adeno-associated viral vectors. Methods 28, 267–275. [PubMed: 12413426]

McKinnon SJ, Lehman DM, Tahzib NG, Ransom NL, Reitsamer HA, Liston P, LaCasse E, Li Q, Korneluk RG, and Hauswirth WW (2004). Beculoviral IAP Repeat-Containing-4 protects optic nerve axons in a rat glaucoma model. Mol Ther 5, 780–787.

Moore DL, Blackmore MG, Hu Y, Kaestner KH, Bixby JL, Lemmon VP, and Goldberg JL (2009). KLF family members regulate intrinsic axon regeneration ability. Science 326, 298–301. [PubMed: 19815778]

Park KK, Liu K, Hu Y, Smith PD, Wang C, Cai B, Xu B, Connolly L, Kramvis I, Sahin M, et al. (2008). Promoting axon regeneration in the adult CNS by modulation of the PTEN/mTOR pathway. Science 322, 963–966. [PubMed: 18988856]

Pearson JT, and Kerschensteiner D (2015). Ambient illumination switches contrast preference of specific retinal processing streams. J Neurophysiol 114, 540–550. [PubMed: 25995351]

Shalata A, Ramirez MC, Desnick RJ, Priedigkeit N, Buettner C, Lindtner C, Mahroum M, Abdul-Ghani M, Dong F, Arar N, et al. (2013). Morbid obesity resulting from inactivation of the ciliary protein CEP19 in humans and mice. Am J Hum Genet 93, 1061–1071. [PubMed: 24268657]

Shen S, Wiemelt AP, McMorris FA, and Barres BA (1999). Retinal ganglion cells lose trophic responsiveness after axotomy. Neuron 23, 285–295. [PubMed: 10399935]

Sheng M, and Greenberg ME (1990). The regulation and function of c-fos and other immediate early genes in the nervous system. Neuron 4, 477–485. [PubMed: 1969743]

Shyh-Chang N, Zhu H, Yvanka de Soysa T, Shinoda G, Seligson MT, Tsanov KM, Nguyen L, Asara JM, Cantley LC, and Daley GQ (2013). Lin28 enhances tissue repair by reprogramming cellular metabolism. Cell 155, 778–792. [PubMed: 24209617]

Siljee JE, Wang Y, Bernard AA, Ersoy BA, Zhang S, Marley A, Von Zastrow M, Reiter JF, and Vaisse C (2018). Subcellular localization of MC4R with ADCY3 at neuronal primary cilia underlies a common pathway for genetic predisposition to obesity. Nat Genet 50, 180–185. [PubMed: 29311635]

Stutzki H, Leibig C, Andreadaki A, Fischer D, and Zeck G (2014). Inflammatory stimulation preserves physiological properties of retinal ganglion cells after optic nerve injury. Front Cell Neurosci 8, 38. [PubMed: 24574973]

Suzuki S, Tachibana M, and Kaneko A (1990). Effects of glycine and GABA on isolated bipolar cells of the mouse retina. J Physiol 421, 645–662. [PubMed: 1693403]

Tauck DL, Frosch MP, and Lipton SA (1988). Characterization of GABA- and glycine-induced currents of solitary rodent retinal ganglion cells in culture. Neuroscience 27, 193–203. [PubMed: 3200439]

Tedeschi A, Dupraz S, Laskowski CJ, Xue J, Ulas T, Beyer M, Schultze JL, and Bradke F (2016). The Calcium Channel Subunit Alpha2delta2 Suppresses Axon Regeneration in the Adult CNS. Neuron 92, 419–434. [PubMed: 27720483]

Thoenen H, and Sendtner M (2002). Neurotrophins: from enthusiastic expectations through sobering experiences to rational therapeutic approaches. Nat Neurosci 5 Suppl, 1046–1050. [PubMed: 12403983]

Vaquero CF, and de la Villa P (1999). Localisation of the GABA(C) receptors at the axon terminal of the rod bipolar cells of the mouse retina. Neurosci Res 35, 1–7. [PubMed: 10555158]

Vong L, Ye C, Yang Z, Choi B, Chua S Jr., and Lowell BB (2011). Leptin action on GABAergic neurons prevents obesity and reduces inhibitory tone to POMC neurons. Neuron 71, 142–154. [PubMed: 21745644]

Wang XW, Li Q, Liu CM, Hall PA, Jiang JJ, Katchis CD, Kang S, Dong BC, Li S, and Zhou FQ (2018). Lin28 Signaling Supports Mammalian PNS and CNS Axon Regeneration. Cell Rep 24, 2540–2552 e2546. [PubMed: 30184489]

Wu D, Hamilton B, Martin C, Gao Y, Ye M, and Yao S (2009). Generation of induced pluripotent stem cells by reprogramming human fibroblasts with the stemgent human TF lentivirus set. J Vis Exp 8, 1553.

Yoshida K, Kawamura K, and Imaki J (1993). Differential expression of c-fos mRNA in rat retina cells: regulation by light/dark cycle. Neuron 10, 1049–1054. [PubMed: 8318229]

Yu J, Vodyanik MA, Smuga-Otto K, Antosiewicz-Bourget J, Frane JL, Tian S, Nie J, Jonsdottir GA, Ruotti V, Stewart R, et al. (2007). Induced pluripotent stem cell lines derived from human somatic cells. Science 318, 1917–1920. [PubMed: 18029452]

Zhu D, Shi S, Wang H, and Liao K (2009). Growth arrest induces primary-cilium formation and sensitizes IGF-1-receptor signaling during differentiation induction of 3T3-L1 preadipocytes. J Cell Sci 122, 2760–2768. [PubMed: 19596798]

Zhu H, Shyh-Chang N, Segre AV, Shinoda G, Shah SP, Einhorn WS, Takeuchi A, Engreitz JM, Hagan JP, Kharas MG, et al. (2011). The Lin28/let-7 axis regulates glucose metabolism. Cell 147, 81–94. [PubMed: 21962509]

Zukor K, Belin S, Wang C, Keelan N, Wang X, and He Z (2013). Short hairpin RNA against PTEN enhances regenerative growth of corticospinal tract axons after spinal cord injury. J Neurosci 33, 15350–15361. [PubMed: 24068802]

- Lin28 overexpression potentiates IGF1 mediated regeneration of injured RGC axons

- Lin28 effects on IGF1 mediated axon regeneration act *via* amacrine cells

- RGC injury hyperactivates amacrine, silencing them allows IGF1 signaling

- RGC primary cilia concentrated IGF1R is lost after injury and reduces IGF1 potency

Zhang et al., find that amacrine cell hyperactivation after RGC axotomy prevents IGF1 responsiveness. Blocking amacrine cell synaptic activity potentiates IGF1 mediated axon regeneration by maintaining IGF1R localization to primary cilia, a localization that is normally lost in injured RGCs.
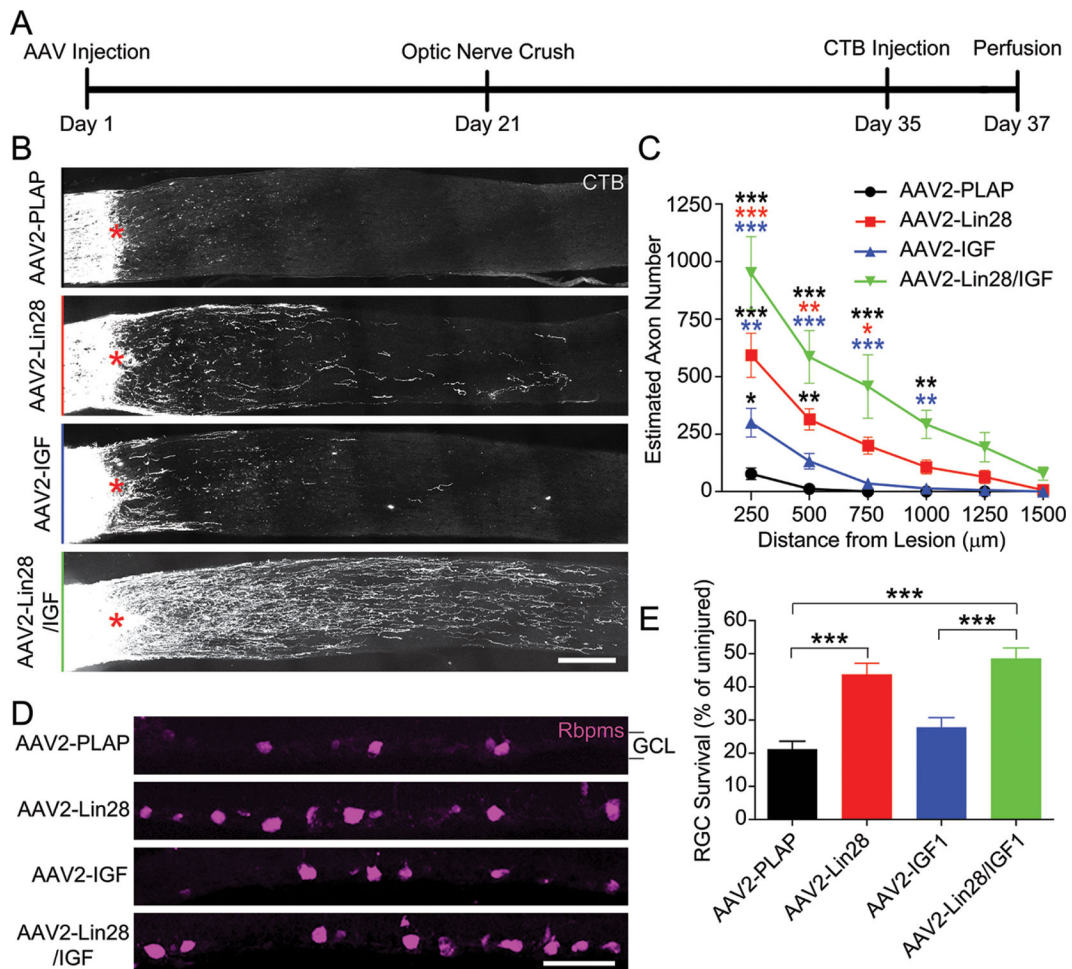
Figure 1. Combinatorial treatment with Lin28 and IGF1 induces robust axon regeneration.
(A) Time course of optic nerve crush and regeneration experiments. (B) Representative confocal image stacks of optic nerve cryosections showing regenerated RGC axons labeled by CTB intraocular injection two weeks after crush in control and treatment conditions. Crush site indicated by red asterisk. (C) Quantification of the extent of RGC axon regeneration in treatment groups. Asterisk colors indicate the group that the p value was significant against (ie. black tested against AAV2-PLAP, red tested again AAV2-Lin28). (D) Representative confocal image stacks of retinal cross-sections stained with the RGC marker Rbpms. (E) Quantification of RGC survival in treatment groups relative to RGC density observed in intact retinas. n = 5–6 mice per group. Scale bar = 200 and 50 μm in panels B and D respectively. *, **, *** p < 0.05, 0.01, 0.001 respectively. See also Figure S1.
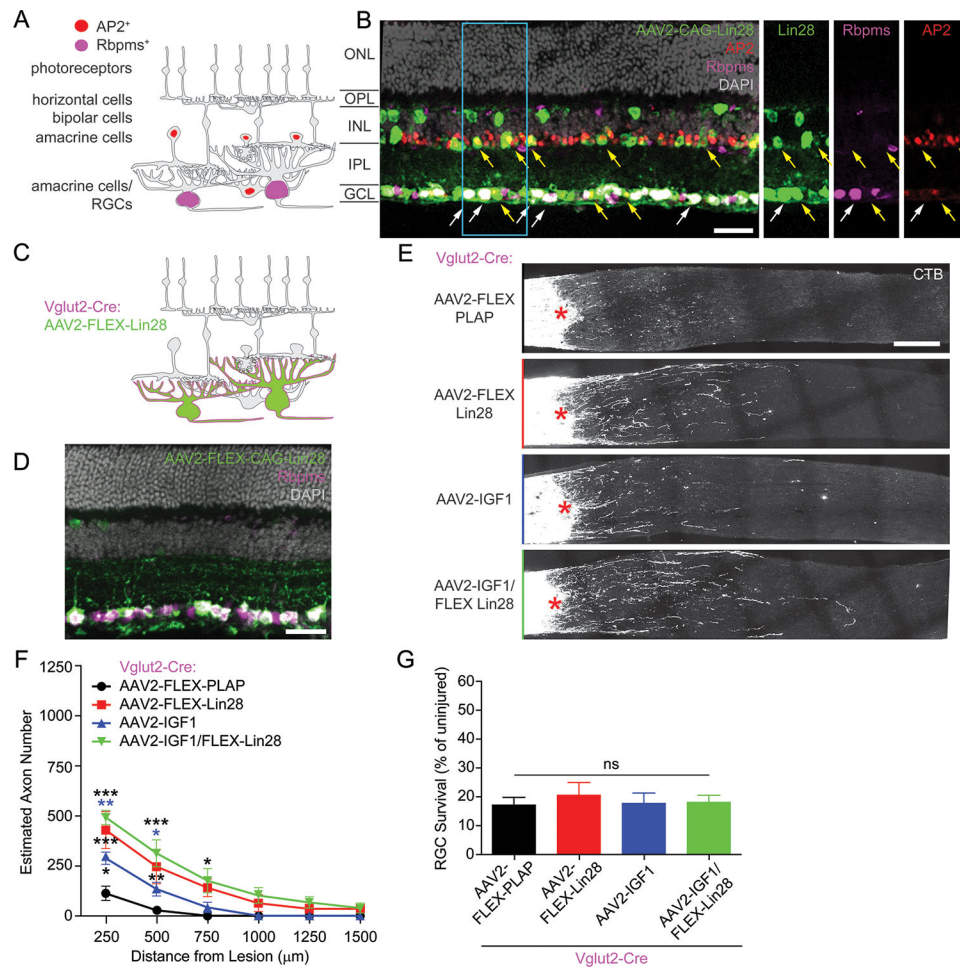
Figure 2. Lin28 mediated axon regeneration is not intrinsic.
(A) Schematic and (B) example confocal image stack demonstrating expression of AAV2-Lin28 in RGCs, amacrine cells and horizontal cells in the intact retina. White arrows indicate Rbpms (magenta) labeled RGCs that express Lin28 (green), while yellow arrows indicated AP2 (red) labeled amacrine cells that express Lin28. Horizontal cell expression was inferred by location and morphology of AP2 negative cells. ONL = outer nuclear layer, OPL = outer plexiform layer, INL = inner nuclear layer, IPL = inner plexiform layer, GCL = ganglion cell layer. (C) Schematic and (D) example confocal image stack showing expression of AAV2-FLEX-Lin28 in the intact Vglut2-Cre transgenic retina where Lin28 expression is restricted to RGCs and sparse horizontal cells. (E) Representative confocal image stacks of CTB labeled RGC axons two weeks after optic nerve crush with RGC restricted expression of Lin28. Asterisks indicate crush site. (F) Quantification of the extent of RGC axon regeneration in treatment groups restricted to RGCs. Asterisk colors indicate the group that the p value was significant against. (G) Quantification of RGC survival relative to RGC density observed in intact retinas in treatment groups restricted to RGCs. Scale bar = 50 mm in panels B and D, and 200 mm in panel E. *, **, *** p < 0.05, 0.01, 0.001 respectively.
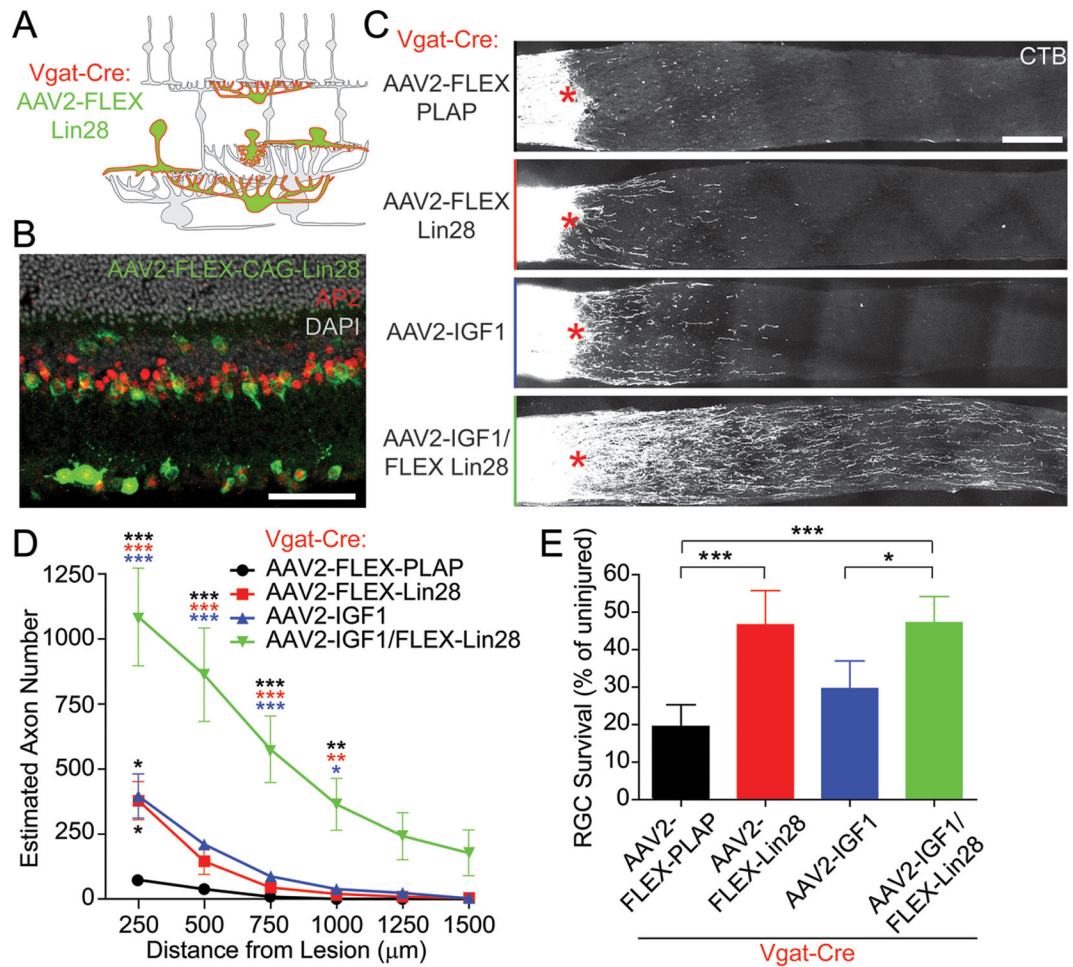
Figure 3. Lin28 expression in inhibitory neurons promotes RGC survival and IGF1-induced axonal regeneration.

(A) Schematic and (B) example confocal image stack showing expression of AAV2-FLEX-Lin28 in the intact Vgat-Cre transgenic retina where Lin28 expression is restricted to amacrine and horizontal cells. (C) Representative confocal image stacks of CTB labeled RGC axons two weeks after optic nerve crush with amacrine cell restricted expression of Lin28. Asterisks indicate crush site. (D) Quantification of the extent of RGC axon regeneration in treatment groups restricted to amacrine cells. Asterisk colors indicate the group that the p value was significant against. (E) Quantification of RGC survival relative to RGC density observed in intact retinas in treatment groups restricted to amacrine cells. n = 5 mice per group. Scale bar = 50 mm in panel B, and 200 mm in panel C. *, **, *** p < 0.05, 0.01, 0.001 respectively. See also Figure S2.
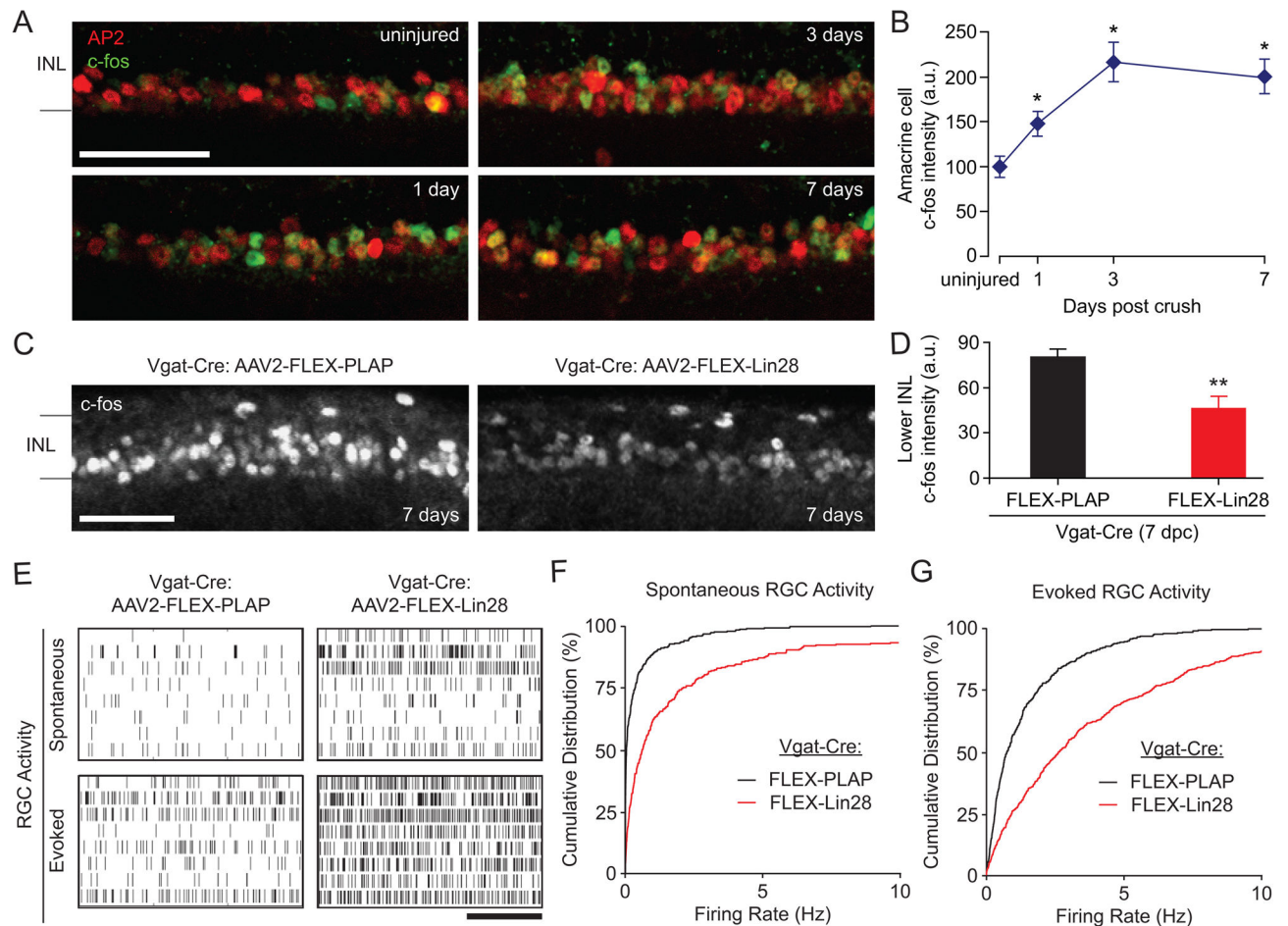
Figure 4. RGC axotomy induced hyperactivation of amacrine cells is inhibited by Lin28 expression.

(A) Confocal image stacks of the INL where AP2 positive amacrine cells (red) are co-labeled with the activity marker c-fos (green) at indicated time points after optic nerve crush in untreated mice. (B) Quantification of c-fos immunostaining intensity in amacrine cells over time after optic nerve crush. n = 6 mice at least 880 cells per group. (C) Confocal images of c-fos expression in the INL of retinas expressing PLAP control (left) or Lin28 in amacrine cells (right) one week after optic nerve crush. (D) Quantification of c-fos immunostaining intensity of cells in the lower INL from the samples exemplified in (c). n = 3 mice per group. (E) Spike trains from RGCs exemplars recorded in dark adapted wholemount retinas using a 128 channel multielectrode array following PLAP control or Lin28 expression in amacrine cells at 6 days after optic nerve crush. Spontaneous activity is presented on the upper plots and light evoked responses to a white noise stimulus on the lower plots. Each row represents activity of a single RGC and each line an action potential. (F, G) Cumulative distribution functions for firing rate of full population of RGCs exemplified in (E) during spontaneous activity (F) and light evoked activity (G) for PLAP (n = 5 mice 108 cells) or Lin28 (n = 6 mice 175 cells) expressing conditions. Scale bar = 50 μm in panels A and C, and 5 s in panel E. *, ** p < 0.05, 0.01 respectively. See also Figures S3 and S4.
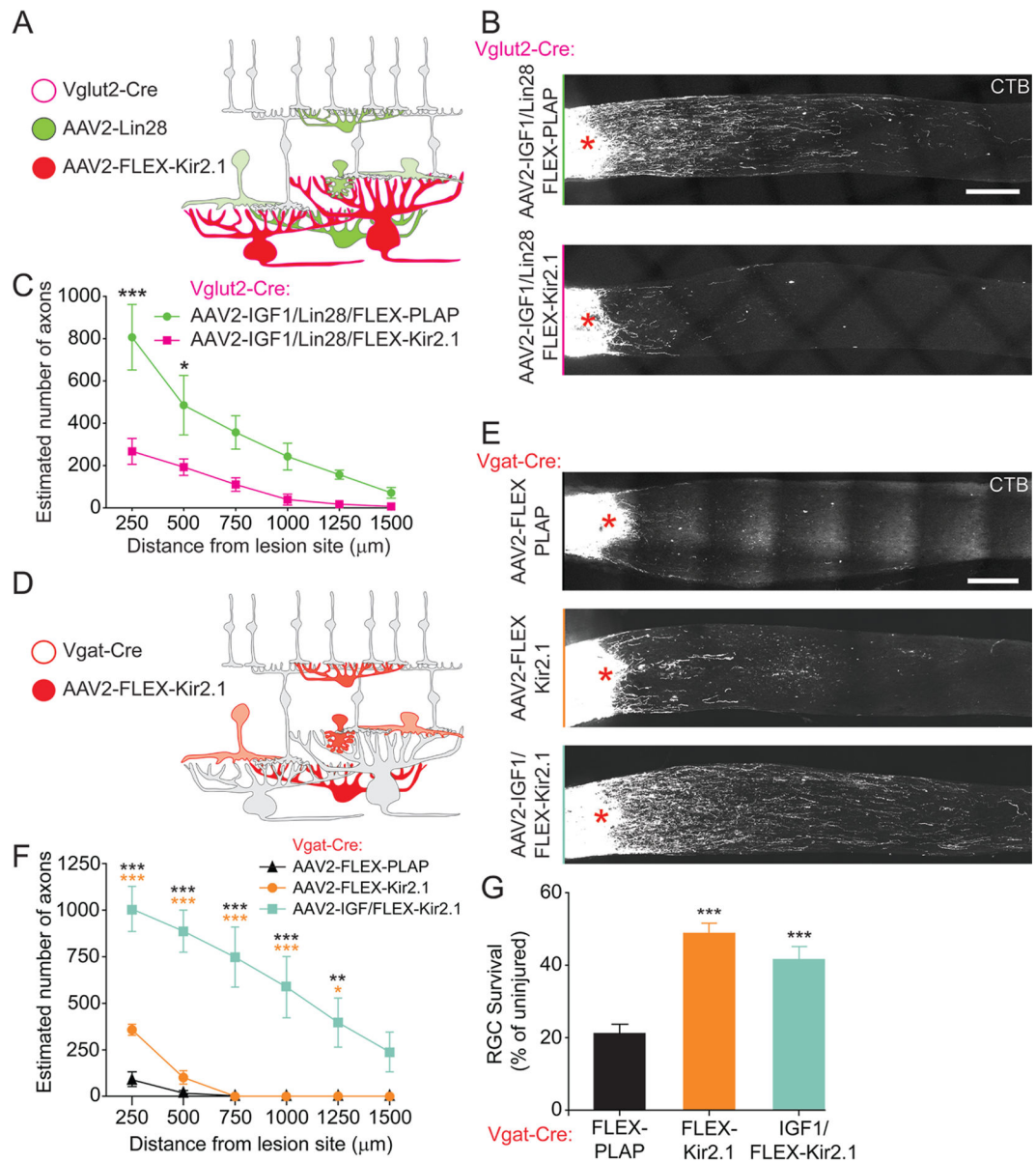
Figure 5. RGC activity is required for, and amacrine cell hyperinhibition prevents Lin28 and IGF1 combinatorial axon regeneration.

(A) Schematic of gene expression used to drive regeneration by widespread delivery of AAV2-IGF1/Lin28 (green), along with RGC specific activity silencing via AAV2-FLEX-Kir2.1 (red) injection into Vglut2-Cre (magenta outline) transgenic mice. (B) Representative confocal image stacks of optic nerve cryosections showing regenerated RGC axons labeled by CTB intraocular injection two weeks after crush in control and treatment conditions. (C) Quantification of the extent of RGC axon regeneration in treatment groups. n = 5 mice per group. Scale bar = 200 mm. *** p < 0.001. (D) Schematic of gene expression used to silence amacrine cells via AAV2-FLEX-Kir2.1 (red) injection into Vgat-Cre (red outline) transgenic mice. (E) Representative confocal image stacks of CTB labeled RGC axons two weeks after optic nerve crush with amacrine cell restricted expression of the inhibitory channel Kir2.1 with and without AAV2-IGF1. (F) Quantification of the extent of axon regeneration
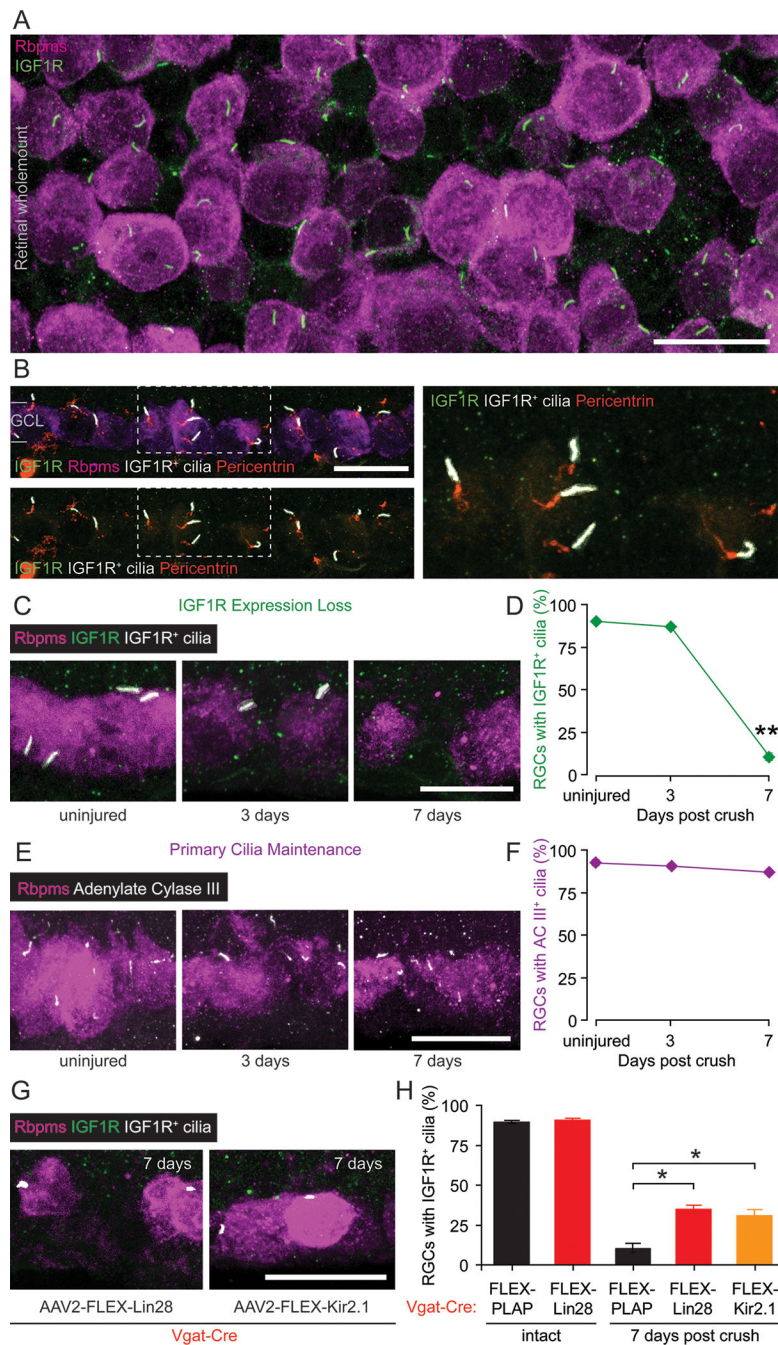
following Kir2.1 mediated amacrine cell silencing. Asterisk colors indicate the group that the p value was significant against. (G) Quantification of RGC survival following Kir2.1 mediated amacrine cell silencing. n = 4–7 mice per group. Scale bar = 200 mm. *, **, *** p < 0.05, 0.01, 0.001 respectively. See also Figure S5.

Figure 6. Injury induced loss of IGF1R enrichment from RGC primary cilia is prevented by Lin28 or Kir2.1 expression in amacrine cells.

(A) Confocal image stack of the GCL from a retinal wholemount immunostained for IGF1R (green) and Rbpms (magenta). (B) Confocal image stack confirming localization of IGF1R to RGC primary cilia. RGCs were immunolabeled for Rbpms and basal bodies with pericentrin antibodies (orange). The lower image is the same as the upper image with the Rbpms signal removed. The image to the right is a zoom in of the boxed region. Ciliary localized IGF1R is pseudocolored in grayscale for clarity. (C) Confocal image stacks of IGF1R expression after injury in Rbpms labeled RGCs. (D) Quantification of RGCs with

maintained cilia localized IGF1R at indicated time points after lesion. n = 4–6 mice at least 120 cells per group. (E) Confocal image stacks of adenylate cyclase III (grayscale) labeled cilia in Rbpms labeled RGCs after injury showing that cilia are not lost in axotomized RGCs. (F) Quantification of RGCs with adenylate cyclase III at indicated time points after lesion. n = 4–6 mice at least 120 cells per group. (G) Representative confocal image stacks showing that some RGCs maintain ciliary expression of IGF1R at 7 days post injury when amacrine cells express either Lin28 or Kir2.1. (H) Quantification of RGCs with maintained IGF1R expression in cilia for indicated conditions. n = 4–6 mice at least 80 cells per groups. Scale bars = 20 mm. * p < 0.05, ** p < 0.01. See also Figure S6.
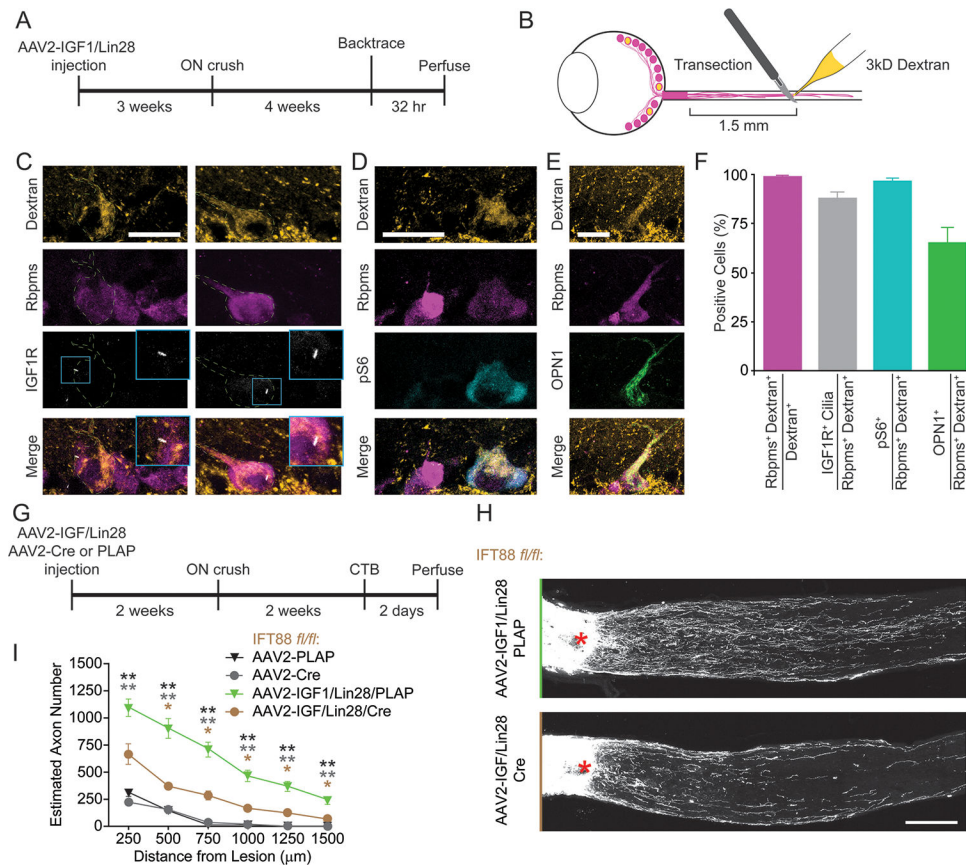
Figure 7. Regenerating RGCs maintain IGF1R expression in their primary cilia.
(A) Time course and (B) schematic of backtracing experiments to label cell bodies of
regenerated RGCs. (C) Example confocal image stacks of dextran (yellow) backtraced
RGCs labeled with Rbpms (magenta) that maintain expression of IGF1R (grayscale) in their
cilia. (D) Example confocal image stack of dextran backtraced RGC labeled with Rbpms
that upregulate phosphorylated S6 (cyan) expression. €Example confocal image stack of
dextran backtraced RGC labeled with the alpha-RGC marker OPN1 (green). (F)
Quantification of the rates for which dextran positive cells were found positive for Rbpms
(magenta), dextran and Rbpms double positive cells were found with IGF1R
immunoreactive cilia (gray), were positive for pS6 (cyan) or OPN1 (green) expression
(cyan) (n = 5 mice 350 cells). (G) Time course of experiments for experiments removing
primary cilia mediated by IFT88 inducible knockout. (H) Representative confocal image
stacks of optic nerve cryosections showing regenerated RGC axons labeled by CTB
intraocular injection two weeks after crush in regeneration and cilia knockout conditions. (I)
Quantification of the extent of RGC axon regeneration in treatment groups. n = 4 mice per
group. Scale bar = 20 mm in panels C and D, and 200 mm in G. * p < 0.05, ** p < 0.01. See
also Figure S7.

KEY RESOURCES TABLE

REAGENT or RESOURCE	SOURCE	IDENTIFIER
Antibodies		
Rabbit anti-Lin28a	Cell Signaling	AB_2297060
Mouse anti-Lin28a	Cell Signaling	AB_1903976
Guinea pig anti-RBPMS	Raygene	Cat# A008712
Rabbit anti-c-Fos	Cell Signaling	AB_2247211
Rabbit anti-IGF1R	Santa Cruz	AB_671788
Rabbit anti-AP2	Abcam	AB_867683
Mouse anti-AP2	Developmental Studies Hybridoma Bank	AB_2313947
Rabbit anti-TrkB	Thermofisher	AB_2736725
Goat anti-osteopontin 1	R&D Systems	AB_354791
Goat anti-choline acetyl transferase	Millipore	AB_2079751
Rabbit anti-pericentrin	Biolegend	AB_2565440
rabbit anti-adenylate cyclase III	Thermofisher	AB_2552692
rabbit anti-phospho S6	Cell Signaling	AB_2181035
Chemicals, Peptides, and Recombinant Proteins		
Alexa-conjugated cholera toxin subunit B	Thermo Fisher Scientific	C34776
Bicuculline	Sigma	14340
imidazoleacetic acid	Sigma	219991
strychnine	Sigma	S0532
recombinant human IGF1	Peprotech	100–11
3 kD dextran conjugated to biotin and TRITC	Thermo Fisher Scientific	D7162
Critical Commercial Assays		
PicoPure RNA Isolation Kit	ThermoFisher	KIT0204
One-Step RT-ddPCR Advanced Kit for Probes	Bio-RAD	1864021
PrimePCR™ ddPCR™ Expression Probe Assay: Tbp, Mouse	Bio-RAD	dMmuCPE5124759
PrimePCR™ ddPCR™ Expression Probe Assay: Grik1, Mouse	Bio-RAD	dMmuCPE5095450
PrimePCR™ ddPCR™ Expression Probe Assay: Gabra1, Mouse	Bio-RAD	dMmuCPE5118172
PrimePCR™ ddPCR™ Expression Probe Assay: Gabrb3, Mouse	Bio-RAD	dMmuCPE5099818
PrimePCR™ ddPCR™ Expression Probe Assay: Kcnh6, Mouse	Bio-RAD	dMmuCPE5115490
PrimePCR™ ddPCR™ Expression Probe Assay: Kcne2, Mouse	Bio-RAD	dMmuCPE5113084
Experimental Models: Organisms/Strains		
Mouse: C57BL/6	Charles River	Strain code#027
Mouse: Vglut2-ires-Cre	Jackson Labs	IMSR_JAX:028863
Mouse: Vgat-ires-Cre	Jackson Labs	IMSR_JAX:016962
Mouse: Connexin 57-Cre	Nicholas Brecha lab from UCLA	N/A
Mouse: IFT88f/f	Jackson Labs	IMSR_JAX:022409
Mouse: IGF1Rf/f	Jackson Labs	IMSR_JAX:012251

REAGENT or RESOURCE	SOURCE	IDENTIFIER
Recombinant DNA		
pAAV-CAG-PLAP	BCH Viral Core	N/A
pAAV-CAG-IGF1	BCH Viral Core	N/A
pAAV-CAG-BDNF	BCH Viral Core	N/A
pAAV-CAG-Lin28a	BCH Viral Core	N/A
pAAV-CAG-NT-3	BCH Viral Core	N/A
pAAV-CAG-FLEX-Lin28a	BCH Viral Core	N/A
pAAV-CAG-FLEX-Kir2.1	BCH Viral Core	N/A
pAAV-CAG-FLEX-GFP	BCH Viral Core	N/A
pAAV-CAG-Cre	BCH Viral Core	N/A
Software and Algorithms		
ImageJ	NIH	RRID: SCR_003070
Prism 7.0	GraphPad Software	RRID: SCR_002798
Plexon Offline Sorter	Plexon Inc.	
Matlab	Mathworks	
Other		
Ultraview Vox Spinning Disk Confocal Microscope	PerkinElmer	N/A
LSM 710 scanning confocal microscope	Zeiss	N/A
256MEA200/30iR-ITO-gr multielectrode array	Multi Channel Systems	
OLED-XL	eMagin	